Published in final edited form as:
Cell Metab. 2012 May 2; 15(5): 778–786. doi:10.1016/j.cmet.2012.03.019.

Elevated PGC-1α Activity Sustains Mitochondrial Biogenesis and Muscle Function without Extending Survival in a Mouse Model of Inherited ALS

Sandrine Da Cruz[1,8], **Philippe A. Parone**[1,8], **Vanda S. Lopes**[4], **Concepción Lillo**[5], **Melissa McAlonis-Downes**[1], **Sandra K. Lee**[1], **Anne P. Vetto**[1], **Susanna Petrosyan**[2], **Martin Marsala**[3,6], **Anne N. Murphy**[2], **David S. Williams**[4], **Bruce M. Spiegelman**[7], and **Don W. Cleveland**[1,*]

[1]Ludwig Institute for Cancer Research and Department of Cellular and Molecular Medicine, University of California, San Diego, La Jolla, CA 92093, USA

[2]Department of Pharmacology, University of California, San Diego, La Jolla, CA 92093, USA

[3]Anesthesiology Research Laboratory, Department of Anesthesiology, University of California, San Diego, La Jolla, CA 92093, USA

[4]Jules Stein Eye Institute and Department of Neurobiology, UCLA School of Medicine, University of California, Los Angeles, 200 Stein Plaza, Los Angeles, CA 90095, USA

[5]Instituto de Neurociencias de Castilla y León, 37007 Salamanca, Spain

[6]Institute of Neurobiology, Slovak Academy of Sciences, Soltesovej 4, Kosice, Slovakia

[7]Dana-Farber Cancer Institute and Department of Cell Biology, Harvard Medical School, Boston, MA 02115, USA

SUMMARY

The transcriptional coactivator PGC-1α induces multiple effects on muscle, including increased mitochondrial mass and activity. Amyotrophic lateral sclerosis (ALS) is a progressive, fatal, adult-onset neurodegenerative disorder characterized by selective loss of motor neurons and skeletal muscle degeneration. An early event is thought to be denervation-induced muscle atrophy accompanied by alterations in mitochondrial activity and morphology within muscle. We now report that elevation of PGC-1α levels in muscles of mice that develop fatal paralysis from an ALS-causing SOD1 mutant elevates PGC-1α-dependent pathways throughout disease course. Mitochondrial biogenesis and activity are maintained through end-stage disease, accompanied by retention of muscle function, delayed muscle atrophy, and significantly improved muscle endurance even at late disease stages. However, survival was not extended. Therefore, muscle is not a primary target of mutant SOD1-mediated toxicity, but drugs increasing PGC-1α activity in muscle represent an attractive therapy for maintaining muscle function during progression of ALS.

*Correspondence: dcleveland@ucsd.edu.
[8]These authors contributed equally to this work

SUPPLEMENTAL INFORMATION

Supplemental Information includes four figures and Supplemental Experimental Procedures and can be found with this article online at doi:10.1016/j.cmet.2012.03.019.

INTRODUCTION

Peroxisome proliferator-activated receptor gamma (PPARγ) co-activator-1α (PGC-1α) is a transcriptional coactivator of nuclear receptors and other transcriptional factors that can enhance multiple aspects of cellular energy metabolism, including mitochondrial biogenesis and angiogenesis (Handschin, 2010). Forced expression of PGC-1α in cultured mammalian cells or specific tissues of transgenic mice increases number and mass of mitochondria together with a strong enhancement of cellular respiratory capacity (Lin et al., 2005). Skeletal muscle-restricted expression of PGC-1α in mice induces a shift from fast glycolytic type IIB muscle fibers toward slow oxidative type I and IIA fibers (Lin et al., 2002), accompanied by altered composition of the presynaptic terminals of neuromuscular junctions (Chakkalakal et al., 2010). PGC-1α in skeletal muscles reduces muscle degeneration following acute denervation (Sandri et al., 2006), regulates expression of components of neuromuscular junctions (Handschin et al., 2007), and induces angiogenesis (Arany et al., 2008).

Amyotrophic lateral sclerosis (ALS) is a progressive adult-onset neurodegenerative disorder that leads to fatal paralysis. Disease in humans and rodent models initiates with muscle denervation and muscle atrophy following denervation, each arising from degeneration and selective loss of motor neurons in the brain and spinal cord. Approximately 10% of human ALS is dominantly inherited, with one-fifth of the familial cases caused by mutations in the ubiquitously expressed Cu, Zn superoxide dismutase (SOD1). In mice, degeneration and death of neurons from the ubiquitously expressed ALS-linked SOD1 mutants arise from acquired toxicity (or toxicities) of the SOD1 mutant proteins and not from loss of enzymatic activity (Bruijn et al., 1998). Extensive work with such mice has supported multiple mutant SOD1-dependent toxicities, as well as the now generally accepted view that motor neuron death may derive from SOD1-mediated toxicities acting within different cell types in the central nervous system, resulting in non-cell-autonomous disease (Ilieva et al., 2009).

Mitochondria have been implicated as a target for toxicity in ALS by several studies reporting decreased mitochondrial Ca^{2+} capacity (Damiano et al., 2006), altered distribution of axonal mitochondria (Vande Velde et al., 2011), abnormal mitochondrial morphology, elevated levels of mitochondrial reactive oxygen species (ROS) production, and deficits in mitochondrial respiration and ATP production in the central nervous system and muscles of ALS patients and mutant SOD1 mice (see Kawamata and Manfredi, 2010 for review). Lending further support to a role for the mitochondria as a target of SOD1 toxicity are findings that mutant SOD1 is enriched in spinal cord mitochondria in ALS mice (see Kawamata and Manfredi, 2010 for review), and it has been proposed to inhibit the activity of multiple mitochondrial components (Israelson et al., 2010; Kawamata et al., 2008; Li et al., 2010; Pedrini et al., 2010).

However, the reports of mitochondrial dysfunctions are inconsistent, and most proposed alterations are not shared among different ALS models. Moreover, while endogenous SOD1 is ubiquitously expressed, muscle-restricted expression of mutant SOD1 in mice has been reported to damage muscle (Dobrowolny et al., 2008; Wong and Martin, 2010) and/or to induce some denervation (Wong and Martin, 2010), albeit without causing ALS-like disease. This has led to the controversial conclusion that muscle is a primary target for SOD1 mutant toxicity (Dobrowolny et al., 2008). Three key questions remain unresolved: (1) is mutant SOD1-dependent damage within the muscle a key contributor to disease, (2) does mitochondrial dysfunction within muscle contribute to muscle and motor neuron degeneration, and (3) can enhanced muscle function and endurance throughout disease slow ALS pathogenesis? We have now tested these questions utilizing mice with elevated PGC-1α expressed selectively in skeletal muscle.

RESULTS

Increased PGC-1α Expression in Mutant SOD1^{G37R} Skeletal Muscles Increases PGC-1α Activity and Mitochondrial Biogenesis/Mass throughout Disease

To determine whether improving muscle function by elevating PGC-1α in skeletal muscles alters SOD1 mutant-mediated ALS disease course and pathogenesis, a SOD1^{G37R} mutant ALS mouse model (Boillée et al., 2006) that develops fatal paralysis by 13–14 months of age was bred with MCK-PGC-1α mice carrying a transgene expressing PGC-1α under the control of the muscle creatine kinase promoter (Lin et al., 2002). PGC-1α mRNA (Figure S1A) and protein (Figure S1B) levels were significantly elevated (e.g., mRNAs were increased 8-fold prior to disease onset and remained 5-fold higher through all symptomatic stages) in the muscles of SOD1^{G37R}/MCK-PGC-1α mice compared to those in SOD1^{G37R} mice.

Increased PGC-1α levels resulted in enhanced PGC-1α activity in SOD1^{G37R}/MCK-PGC-1α mice, as indicated by elevation of RNA transcripts from genes known to be targets of PGC-1α. These genes included those coding for (1) mitochondrial proteins (COX4, cytochrome *c* oxidase subunit IV; Cytc, cytochrome *c*; and UCP2, uncoupling protein 2), (2) the angiogenic vascular endothelial growth factor (VEGF), (3) the hydrogen peroxide detoxifying enzyme catalase, and (4) the mitochondrial superoxide dismutase (SOD2) (Figures 1A, S1C, and S1D). Of note, elevated expression of PGC-1α in skeletal muscle of SOD1^{G37R} mice did not alter the level of SOD1 (Figure S1E). Elevated PGC-1α activity drove an increase in acetylcholine receptor (AChR) clustering in the gastrocnemius of SOD1^{G37R}/MCK-PGC-1α mice (measured by counting AChR clusters per muscle section at 4 and 13–14 months of age, with SOD1^{G37R}/MCK-PGC-1α: 91.8 ± SEM 5.8 and 89.9 ± SEM 8.2 AChR clusters, respectively, and SOD1^{G37R}: 69 ± SEM 5.5 and 61.9 ± SEM 1.6) (Figure 1B). Importantly, the effects of increased PGC-1α activity were sustained throughout disease (Figures 1 and S1).

Quantification of electron microscopic images of tibialis anterior muscles revealed a combined increase in mitochondrial number and area per mitochondrion that yielded a 3- to 4-fold elevation of the total area of mitochondria per myofiber in SOD1^{G37R}/MCK-PGC-1α mice (Figures 1C, 1D, and S1F) prior to disease onset and that was sustained through end-stage disease (Figure 1D). Cristae of the larger mitochondria in SOD1^{G37R}/MCK-PGC-1α mice appeared morphologically normal. Notably, despite decline in total levels of PGC-1α at disease end-stage in SOD1^{G37R}/MCK-PGC-1α muscles to levels near those from age-matched nontransgenic animals (Figure S1B), a 3-fold increase in mitochondrial mass and elevation of RNA transcripts from genes known to be targets of PGC-1α (including catalase, SOD2, and UCP2) (Figures 1 and S1) was continued to end-stage disease.

Selective Expression of PGC-1α in Mutant SOD1^{G37R} Skeletal Muscles Improves Muscle Endurance and Performance

Known activities of PGC-1α in muscle include converting muscle fibers to a slow phenotype (Lin et al., 2002) that is known to undergo denervation later in SOD1-mediated disease (Frey et al., 2000) and inducing retrograde changes at the neuromuscular junctions (Chakkalakal et al., 2010). To determine whether increased PGC-1α activity and enhanced mitochondrial biogenesis/mass altered muscle function of SOD1^{G37R}/MCK-PGC-1α transgenic mice, resistance to fatigue was assessed throughout disease by electrical stimulation of hindlimb muscles to mimic repeated contractions occurring during exercise. Endurance of the muscle was expressed as a fatigue index corresponding to the time (seconds) required for the muscle contraction amplitude to fall below 50% of the starting level (Lin et al., 2002). Muscle-specific increased expression of PGC-1α in SOD1^{G37R} mice

produced a sustained increase in resistance to fatigue of hindlimb muscles in asymptomatic and symptomatic SOD1^{G37R}/MCK-PGC-1α mice (reflected in a significantly higher fatigue index; Figures 2A, S2A, and S2B) that remained 3-fold higher than in SOD1^{G37R} animals even at end-stage disease (303 ± SEM 34 s versus 92 ± SEM 17 s, respectively).

Overall locomotor performance of symptomatic SOD1^{G37R}/MCK-PGC-1α versus SOD1^{G37R} mice was also tested on an inclined treadmill by progressively increasing running speeds until exhaustion. Here again, SOD1^{G37R}/MCK-PGC-1α mice consistently displayed a significant increase in performance, as shown by almost two times longer distances covered per run compared with SOD1^{G37R} animals (Figures 2B and S2C; SOD1^{G37R}/MCK-PGC-1α: 48 ± SEM 4.4 min, 792 ± SEM 99 m and SOD1^{G37R}: 31 ± SEM 3 min, 442 ± SEM 57 m).

To further determine whether the increased muscle function improved locomotor activity in performing voluntary tasks, symptomatic animals were tested on a running wheel and in an open field test. For the first test, mice were placed in a closed running wheel and their performance (without further stimulation) was monitored over 5 min. SOD1^{G37R}/MCK-PGC-1α mice ran significantly (almost three times) longer (2.8 ± SEM 0.3 min versus 1.0 ± SEM 0.2 min) and covered more than three times longer distances (24 ± SEM 3.7 m versus 6.9 ± SEM 2.0 m, respectively) compared with symptomatic SOD1^{G37R} animals (Figure 2C). Finally, to assess spontaneous and voluntary locomotor activity, open field movement was recorded for 60 min. SOD1^{G37R}/MCK-PGC-1α animals were mobile longer than SOD1^{G37R} mice (19 ± SEM 1.4 min versus 12.5 ± SEM 1.8 min) and covered a larger distance (66 ± SEM 6 m versus 42 ± SEM 7.1 m) (Figure 2D). The average speed of both sets of animals was not significantly different in either running wheel or open field tests.

Overall, we conclude that increasing PGC-1α activity and enhancing mitochondrial biogenesis/mass in skeletal muscles of SOD1^{G37R} mice leads to a significant increase in muscle endurance, resulting in markedly improved locomotor activity at symptomatic stages of ALS disease.

Increased Expression of PGC-1α in Mutant SOD1^{G37R} Skeletal Muscles Reduces Muscle Degeneration and Increases Mitochondrial ATP Producing Capacity

A classical hallmark of ALS pathogenesis is grouped muscle atrophy and degeneration. At asymptomatic stages (4 months), no significant differences were found in muscle structure or fiber cross-sectional area of muscle in SOD1^{G37R} or SOD1^{G37R}/MCK-PGC-1α animals (Figures 3A, 3B, S3D, and S3E). At symptomatic ages, while average muscle fiber size and distribution in the gastrocnemius decreased sharply in SOD1^{G37R} mice, expression of PGC-1α prevented muscle atrophy in SOD1^{G37R}/MCK-PGC-1α animals (894 ± SEM 27 μm^2 versus 1393 ± SEM 100 μm^2, respectively; Figures 3A, 3B, and S3A). Even at end-stage, muscle atrophy in SOD1^{G37R}/MCK-PGC-1α was still significantly reduced compared with SOD1^{G37R} animals (1141 ± SEM 66 μm^2 versus 878 ± SEM 63 μm^2 in the gastrocnemius [Figure 3B], with similar results in the plantaris [Figures S3B and S3C]).

PGC-1α was previously shown (Sandri et al., 2006) to inhibit expression of genes involved in muscle degeneration (including those encoding the ubiquitin ligase MuRF-1 and the lysosomal hydrolase cathepsin L) following nerve crush-induced denervation. To determine whether PGC-1α prevented muscle atrophy through a similar mechanism during SOD1 mutant-derived disease, we determined mRNA levels for MuRF-1 and cathepsin L. Levels of both degeneration markers significantly increased (Figures 3C and S3F) at the symptomatic stage of disease in SOD1^{G37R} animals (MuRF-1: 0.38 ± SEM 0.04 and cathepsin L: 0.24 ± SEM 0.04 n = 3 at 4 months compared with 0.73 ± SEM 0.07 and 0.48 ± SEM 0.01, respectively, at 12 months). However, this disease-dependent increase in both

MuRF-1 and cathepsin L mRNAs was significantly reduced in the gastrocnemius of disease-matched SOD1^{G37R}/MCK-PGC-1α mice (MuRF-1: 0.33 ± SEM 0.07 and cathepsin L: 0.21 ± SEM 0.002 n = 3 at 4 months compared with 0.42 ± SEM 0.01 and 0.36 ± SEM 0.03, respectively, at 12 months).

Since mitochondrial biogenesis and mass were significantly increased throughout disease in muscle of the SOD1^{G37R}/MCK-PGC-1α mice (Figure 1), we tested if increased PGC-1α expression improved muscle function by increasing mitochondrial energy-producing capacity, thereby making more ATP available for sustained muscle activity. Measurement of mitochondrial ADP phosphorylation capacity per milligram of muscle (measured by determining the rate of mitochondrial oxygen consumption while ADP is being phosphorylated to ATP) revealed a 2.5-fold higher capacity in SOD1^{G37R}/MCK-PGC-1α mice compared with SOD1^{G37R} animals (Figure 3D).

Altogether, our findings indicate that improved muscle function and endurance that is sustained throughout disease in SOD1^{G37R}/MCK-PGC-1α mice results from a combination of PGC-1α-dependent reduction in muscle atrophy (Figures 3A–3C), increased VEGF levels (Figure 1A), and increased energy supply from the mitochondria (Figures 1C, 1D, and 3D).

Improving Muscle Function by Elevating Levels of PGC-1α in SOD1^{G37R} Animals Does Not Delay Neurodegeneration

We determined whether the sustained improvement in muscle function during disease by increasing PGC-1α in the muscles of SOD1^{G37R} animals altered disease course by following disease in cohorts of SOD1^{G37R} and SOD1^{G37R}/MCK-PGC-1α animals (n ≥ 30). No changes were found in age of disease onset (244 ± SEM 4 versus 242 ± SEM 4 days, respectively), age of reaching the symptomatic stage (366 ± SEM 4 versus 359 ± SEM 5 days), and survival (395 ± SEM 5 versus 388 ± SEM 4 days) (Figure 4A). Additional hallmarks of ALS pathogenesis were also unaffected by sustained PGC-1α-driven improvement in muscle function, including the percentages of innervated neuromuscular junctions at all disease stages (Figure 4B) (with 47% and 53%, respectively, of junctions in the gastrocnemius muscle denervated at onset in SOD1^{G37R} and SOD1^{G37R}/MCK-PGC-1α mice, 72% and 75% denervation at symptomatic stage, and 81% and 85% denervation at end-stage disease).

Similarly, there were no significant differences in α-motor axon loss at onset or during disease course (Figure 4C) or cholinergic ventral horn motor neuron death (Figures 4D and S4). Nor were there differences in the increased level of astroglial and microglial activation markers (GFAP and Iba1, respectively; Figure 4E) in the spinal cord ventral horns of SOD1^{G37R} and SOD1^{G37R}/MCK-PGC-1α animals. Altogether, while muscle function was enhanced early in disease and remained so throughout disease in SOD1^{G37R} mice by elevating expression of PGC-1α in muscle, initiation and continuance of neurodegeneration, including loss of motor axons and death of motor neurons, was completely unaffected.

DISCUSSION

Understanding the contribution of muscle in ALS has important practical implications in treating disease. Reports of mitochondrial dysfunction in muscles of ALS mouse models and in patients (see Dupuis, 2009 for review) have suggested that mitochondria within the muscle may play a critical role in ALS pathogenesis. Muscle-restricted expression of mutant SOD1 (as opposed to the ubiquitous expression of endogenous SOD1 that causes paralytic disease) has been reported to induce muscle atrophy, muscle mitochondrial dysfunction, reduced muscle strength, and muscle damage (Dobrowolny et al., 2008; Wong and Martin, 2010) and/or to induce some denervation (Wong and Martin, 2010). There are major

discrepancies between these two reports. One study (Dobrowolny et al., 2008) reported that damage to the muscle is mutant SOD1 specific and is not accompanied by evident signs of motor neuron degeneration, while another (Wong and Martin, 2010) reported that both wild-type and mutant SOD1 expression in muscle leads to muscle damage as well as neuronal degeneration. In neither report did muscle-restricted mutant SOD1 cause ALS-like disease in mice; nevertheless, both studies concluded that skeletal muscle is a primary target of SOD1-mediated toxicity.

Our evidence refutes such a conclusion, demonstrating to the contrary that sustained improvement in muscle activity, including a doubling in endurance, increased energy supply from the mitochondria in muscles, and reducing muscle atrophy throughout ALS-like disease, does not prevent or delay retraction of the axons from neuromuscular junctions, loss of motor axons, or death of motor neurons. If muscle atrophy/dysfunction in ALS induced a toxic signal(s) to motor neurons, preventing muscle degeneration through enhanced expression of PGC-1α should have reduced such a toxic signal leading to delay in disease onset/progression. This was not the case. Moreover, earlier evidence had shown that selectively lowering synthesis in muscle (either by viral-delivered siRNA or by selective deletion of a mutant SOD1 transgene solely in muscle) of ubiquitously expressed mutant SOD1 did not alter any aspect of neurodegeneration in animals that do develop fatal paralytic disease (Miller et al., 2006). Similarly, increasing muscle mass and strength prior to disease onset and through the early disease phase (by injection of myostatin antibodies into SOD1 mutant mice [Holzbaur et al., 2006]) or through to end stage disease (by viral delivery of the myostatin-inhibitor follistatin [Miller et al., 2006]) did not affect disease course. When combined with our evidence, it is now clear that SOD1 mutant damage within muscle is not an important contributor to the pathogenic process through which ubiquitously expressed ALS-linked SOD1 mutants provoke age-dependent degeneration and death of motor neurons and the subsequent fatal paralysis.

Muscle weakness is, nevertheless, a characteristic symptom in ALS patients and leads to reduced physical activity, which progresses into muscle disuse-induced atrophy and cardiovascular deconditioning. Here we have demonstrated that increasing PGC-1α activity in the muscles of SOD1 mutant-expressing mice produces significantly increased muscle endurance, reduced atrophy, and improved locomotor activity, even at late stages of disease, without extending survival. To earlier evidence that elevated PGC-1α can protect skeletal muscles from atrophy following acute denervation by directly interfering with a FoxO3-dependent pathway (Sandri et al., 2006), here we add that PGC-1α significantly reduces muscle atrophy throughout SOD1 mutant-dependent disease, concomitant with decreased induction of FoxO3 target genes (*cathepsin L* and *MuRF1*) and increased muscle ATP output, expression of VEGF, and acetylcholine receptor clustering. We conclude that the improved muscle activity in mutant SOD1 mice expressing PGC-1α results from modulation of multiple PGC-1α responsive pathways, including an enhancement in mitochondrial biogenesis and an inhibition of the FoxO3-dependent protein degradation pathway.

Therefore, improving muscle activity and reducing atrophy may be effective to improve or preserve daily functioning and quality of life for ALS patients. We propose that compounds inducing PGC-1α expression, delivered systemically or applied specifically to the muscle, could be used as a palliative treatment in ALS patients to increase muscle function, reduce atrophy, and improve daily physical activity, thus resulting in a better quality of life for patients.

EXPERIMENTAL PROCEDURES

Animals

MCK-PGC-1α mice are mice heterozygous for PGC-1α cDNA under the control of muscle creatine kinase promoter (Lin et al., 2002). LoxSOD1^{G37R} ALS mice are mice heterozygous for a 12 kb genomic DNA fragment encoding the human SOD1^{G37R} transgene, under its endogenous promoter, flanked by loxP sequences (Boillée et al., 2006). All transgenic mouse lines were on a pure C57BL/6 background.

Quantitative Real-Time PCR

mRNA levels were determined by quantitative real-time PCR using the iQSYBR Green supermix (Bio-Rad, Hercules, CA).

Immunoblotting

PGC-1α was immunoprecipitated using a rabbit anti-PGC-1α antibody (Santa Cruz; H300) from the gastrocnemius muscle of nontransgenic and MCK-PGC-1α mice. The immunoprecipitated proteins were separated on SDS-PAGE, transferred to nitrocellulose membranes, and probed with PGC-1α antibody (Calbiochem; 4C1.3).

Immunofluorescence

Cryosections from paraformaldehyde-fixed tissues were stained with the indicated antibodies. Neuromuscular junctions were considered denervated when synaptophysin staining covered less than 50% of the area of α-bungarotoxin staining. A total of approximately 1,000 neuromuscular junctions were counted from at least ten sections of muscle per animal. ChAT-positive ventral horn motor neurons were counted from 25–35 lumbar spinal cord cryosections (per animal) spaced 360 μm apart and expressed as the average motor neurons per section of spinal cord.

Electron Microscopy

Ultrathin sections (70 nm) from the center of EPON-embedded tibialis anterior were stained with 1% uranyl acetate. Images were taken from the center of 15–25 randomly chosen myofibers, and the area of all the mitochondria in each image was determined using ImageJ software. On average, 200–300 mitochondria were analyzed per muscle.

Muscle Histology

Ten micron cryosections of hindlimb muscle (composed of gastrocnemius, soleus, and plantaris) were stained with hematoxylin and eosin, and muscle fiber area in the gastrocnemius or plantaris was determined using ImageJ software on three randomly chosen fields for each muscle.

Morphometric Analysis of Axons

Thin sections (0.75 μm) from EPON-embedded L5 lumbar roots were stained with toluidine blue. The number of large-caliber axons with diameters over 3.5 μm (considered to be α-motor axons) was determined using the Bioquant Software.

Muscle Endurance Measurement

In anesthetized animals, the tibialis anterior muscle was electrically stimulated, and the movement of the hindpaw following muscle contraction was measured by a force transducer. Muscle endurance was expressed as a fatigue index corresponding to the time (in

seconds) required for the amplitude of muscle contraction upon 2 Hz electrical stimulation to fall below 50% of the starting level.

Testing of Locomotor Activity

All testing of locomotor activity was carried out during the animal's dark cycle under red light. Naive mice were run on an enclosed-chamber modular treadmill (Columbus Instruments) with a 5° incline at an initial velocity of 8 m/min. Velocity was increased by 2 m/min every 5 min until exhaustion. Exhaustion was determined to be the point at which the animal would not resume running when provoked through two consecutive 5 s stimulation on a low-voltage power grid. The spontaneous locomotor activity of animals was assessed in an open field (open top plexiglass box of 12 × 12 inches) for 1 hr and analyzed over the test period using the ANY-maze video tracking software. Habituated mice were tested on an activity wheel (Lafayette Instruments) in three 5 min sessions separated by at least 15 min. Running time and distance traveled were determined using a cyclocomputer (Cordless 7; CAT EYE attached to the running wheel detecting the revolution of the wheel with digital magnetic counters) and averaged over the three 5 min test sessions. Activity of the mice was restricted on the wheel. All behavioral studies were performed with the genotype unknown to the examiner.

Mitochondrial Oxygen Consumption

Mitochondrial O_2 consumption was measured using isolated mitochondria from gastrocnemius at 37°C using a Clarke type electrode (Oxytherm, Hansatech Inc.). The rate of pyruvate-stimulated mitochondrial O_2 consumption was multiplied by the total mass of mitochondria per muscle to obtain the rate of oxygen consumption per milligram of muscle.

Statistical Analysis

All data are presented as mean ± SEM. The statistical difference between two individual groups was assessed using the Student's t test; $p < 0.05$ was considered significant.

Supplementary Material

Refer to Web version on PubMed Central for supplementary material.

Acknowledgments

We are very grateful to Prof. Randal Johnson for the use his treadmill apparatus. This work has been supported by grants from the Muscular Dystrophy Association and the NIH to D.W.C. S.D.C. was supported by a postdoctoral fellowship from the ALS Association. Salary support for D.W.C. is provided by the Ludwig Institute for Cancer Research. Support from the NIH and an RPB Jules and Doris Stein Professorship was also provided to D.S.W.

REFERENCES

Arany Z, Foo SY, Ma Y, Ruas JL, Bommi-Reddy A, Girnun G, Cooper M, Laznik D, Chinsomboon J, Rangwala SM, et al. HIF-independent regulation of VEGF and angiogenesis by the transcriptional coactivator PGC-1alpha. Nature. 2008; 451:1008–1012. [PubMed: 18288196]

Boillée S, Yamanaka K, Lobsiger CS, Copeland NG, Jenkins NA, Kassiotis G, Kollias G, Cleveland DW. Onset and progression in inherited ALS determined by motor neurons and microglia. Science. 2006; 312:1389–1392. [PubMed: 16741123]

Bruijn LI, Houseweart MK, Kato S, Anderson KL, Anderson SD, Ohama E, Reaume AG, Scott RW, Cleveland DW. Aggregation and motor neuron toxicity of an ALS-linked SOD1 mutant independent from wild-type SOD1. Science. 1998; 281:1851–1854. [PubMed: 9743498]

Chakkalakal JV, Nishimune H, Ruas JL, Spiegelman BM, Sanes JR. Retrograde influence of muscle fibers on their innervation revealed by a novel marker for slow motoneurons. Development. 2010; 137:3489–3499. [PubMed: 20843861]

Damiano M, Starkov AA, Petri S, Kipiani K, Kiaei M, Mattiazzi M, Flint Beal M, Manfredi G. Neural mitochondrial Ca2+ capacity impairment precedes the onset of motor symptoms in G93A Cu/Zn-superoxide dismutase mutant mice. J. Neurochem. 2006; 96:1349–1361. [PubMed: 16478527]

Dobrowolny G, Aucello M, Rizzuto E, Beccafico S, Mammucari C, Boncompagni S, Belia S, Wannenes F, Nicoletti C, Del Prete Z, et al. Skeletal muscle is a primary target of SOD1G93A-mediated toxicity. Cell Metab. 2008; 8:425–436. [PubMed: 19046573]

Dupuis L. Oxidative stress sensitivity in ALS muscle cells. Exp. Neurol. 2009; 220:219–223. [PubMed: 19733171]

Frey D, Schneider C, Xu L, Borg J, Spooren W, Caroni P. Early and selective loss of neuromuscular synapse subtypes with low sprouting competence in motoneuron diseases. J. Neurosci. 2000; 20:2534–2542. [PubMed: 10729333]

Handschin C. Regulation of skeletal muscle cell plasticity by the peroxisome proliferator-activated receptor γ coactivator 1α. J. Recept. Signal Transduct. Res. 2010; 30:376–384. [PubMed: 20178454]

Handschin C, Kobayashi YM, Chin S, Seale P, Campbell KP, Spiegelman BM. PGC-1alpha regulates the neuromuscular junction program and ameliorates Duchenne muscular dystrophy. Genes Dev. 2007; 21:770–783. [PubMed: 17403779]

Holzbaur EL, Howland DS, Weber N, Wallace K, She Y, Kwak S, Tchistiakova LA, Murphy E, Hinson J, Karim R, et al. Myostatin inhibition slows muscle atrophy in rodent models of amyotrophic lateral sclerosis. Neurobiol. Dis. 2006; 23:697–707. [PubMed: 16837207]

Ilieva H, Polymenidou M, Cleveland DW. Non-cell autonomous toxicity in neurodegenerative disorders: ALS and beyond. J. Cell Biol. 2009; 187:761–772. [PubMed: 19951898]

Israelson A, Arbel N, Da Cruz S, Ilieva H, Yamanaka K, Shoshan-Barmatz V, Cleveland DW. Misfolded mutant SOD1 directly inhibits VDAC1 conductance in a mouse model of inherited ALS. Neuron. 2010; 67:575–587. [PubMed: 20797535]

Kawamata H, Manfredi G. Mitochondrial dysfunction and intracellular calcium dysregulation in ALS. Mech. Ageing Dev. 2010; 131:517–526. [PubMed: 20493207]

Kawamata H, Magrané J, Kunst C, King MP, Manfredi G. Lysyl-tRNA synthetase is a target for mutant SOD1 toxicity in mitochondria. J. Biol. Chem. 2008; 283:28321–28328. [PubMed: 18715867]

Li Q, Vande Velde C, Israelson A, Xie J, Bailey AO, Dong MQ, Chun SJ, Roy T, Winer L, Yates JR, et al. ALS-linked mutant superoxide dismutase 1 (SOD1) alters mitochondrial protein composition and decreases protein import. Proc. Natl. Acad. Sci. USA. 2010; 107:21146–21151. [PubMed: 21078990]

Lin J, Wu H, Tarr PT, Zhang CY, Wu Z, Boss O, Michael LF, Puigserver P, Isotani E, Olson EN, et al. Transcriptional co-activator PGC-1 alpha drives the formation of slow-twitch muscle fibres. Nature. 2002; 418:797–801. [PubMed: 12181572]

Lin J, Handschin C, Spiegelman BM. Metabolic control through the PGC-1 family of transcription coactivators. Cell Metab. 2005; 1:361–370. [PubMed: 16054085]

Miller TM, Kim SH, Yamanaka K, Hester M, Umapathi P, Arnson H, Rizo L, Mendell JR, Gage FH, Cleveland DW, Kaspar BK. Gene transfer demonstrates that muscle is not a primary target for non-cell-autonomous toxicity in familial amyotrophic lateral sclerosis. Proc. Natl. Acad. Sci. USA. 2006; 103:19546–19551. [PubMed: 17164329]

Pedrini S, Sau D, Guareschi S, Bogush M, Brown RH Jr, Naniche N, Kia A, Trotti D, Pasinelli P. ALS-linked mutant SOD1 damages mitochondria by promoting conformational changes in Bcl-2. Hum. Mol. Genet. 2010; 19:2974–2986. [PubMed: 20460269]

Sandri M, Lin J, Handschin C, Yang W, Arany ZP, Lecker SH, Goldberg AL, Spiegelman BM. PGC-1alpha protects skeletal muscle from atrophy by suppressing FoxO3 action and atrophy-specific gene transcription. Proc. Natl. Acad. Sci. USA. 2006; 103:16260–16265. [PubMed: 17053067]

Vande Velde C, McDonald KK, Boukhedimi Y, McAlonis-Downes M, Lobsiger CS, Bel Hadj S, Zandona A, Julien JP, Shah SB, Cleveland DW. Misfolded SOD1 associated with motor neuron mitochondria alters mitochondrial shape and distribution prior to clinical onset. PLoS ONE. 2011; 6:e22031. [PubMed: 21779368]

Wong M, Martin LJ. Skeletal muscle-restricted expression of human SOD1 causes motor neuron degeneration in transgenic mice. Hum. Mol. Genet. 2010; 19:2284–2302. [PubMed: 20223753]

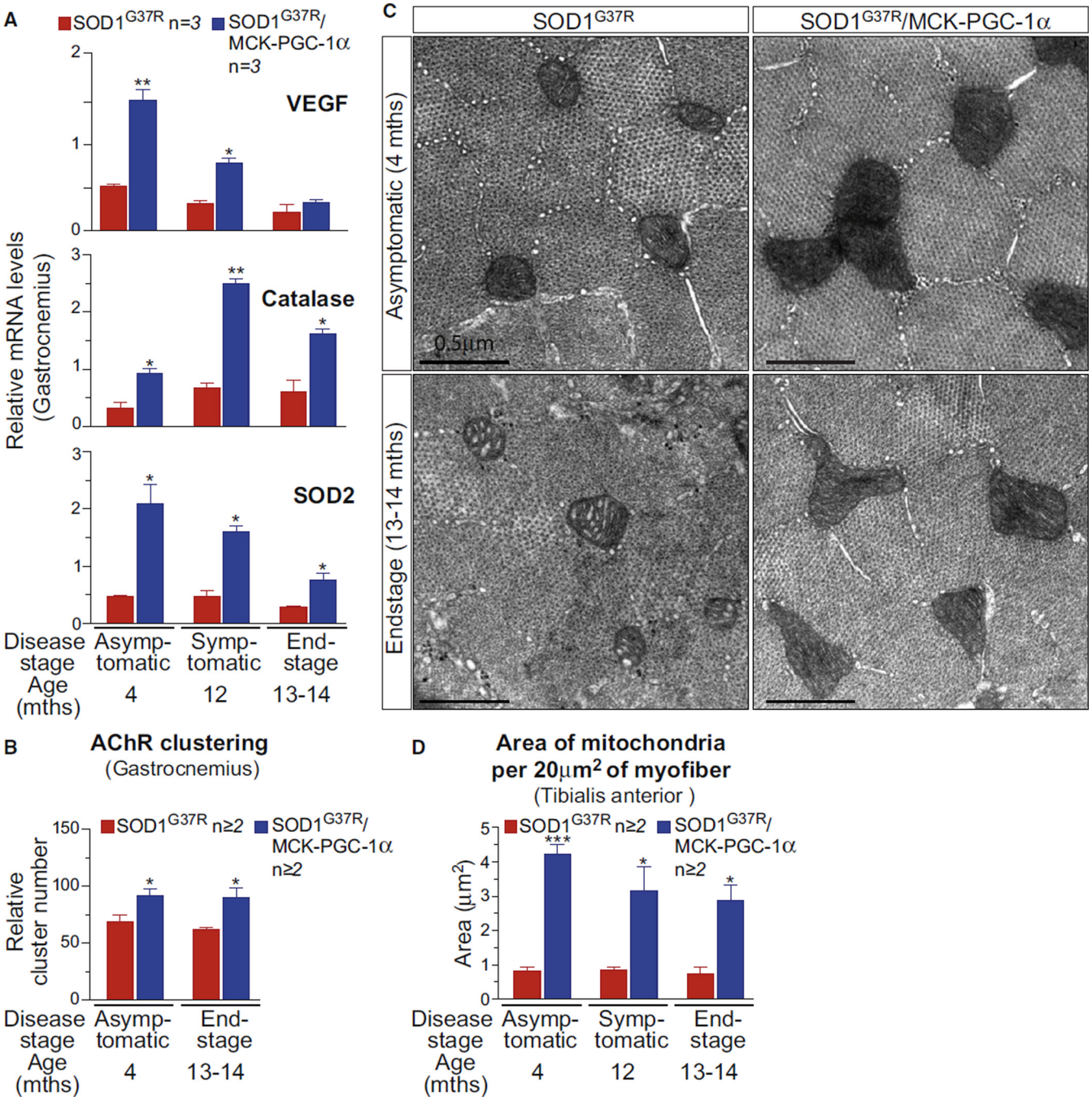

Figure 1. Elevating PGC-1α Expression Activates Known PGC-1α Responsive Pathways, Including Mitochondrial Biogenesis in Skeletal Muscles of SOD1^{G37R} Mutant Mice throughout Disease

(A) Relative mRNA expression levels were determined by quantitative real-time PCR for VEGF, catalase, and SOD2 in gastrocnemius isolated from SOD1^{G37R} and SOD1^{G37R}/ MCK-PGC-1α animals throughout disease. Data are presented as mean ± SEM. See also Figure S1.

(B) Relative numbers of acetylcholine receptor (AChR) clusters per section of gastrocnemius were determined by staining with α-bungarotoxin. Data are presented as mean ± SEM.

(C) Electron micrographs from cross-sections taken from tibialis anterior muscle of $SOD1^{G37R}$ and $SOD1^{G37R}$/MCK-PGC-1α animals at asymptomatic (4 months) and end-stage of disease (13–14 months). Scale bar = 0.5 μm.
(D) Total area of mitochondria per 20 μm^2 of myofiber from tibialis anterior muscle of $SOD1^{G37R}$ and $SOD1^{G37R}$/MCK-PGC-1α animals at asymptomatic (4 months), symptomatic (12 months), and end-stage of disease (13–14 months). Data are presented as mean ± SEM.

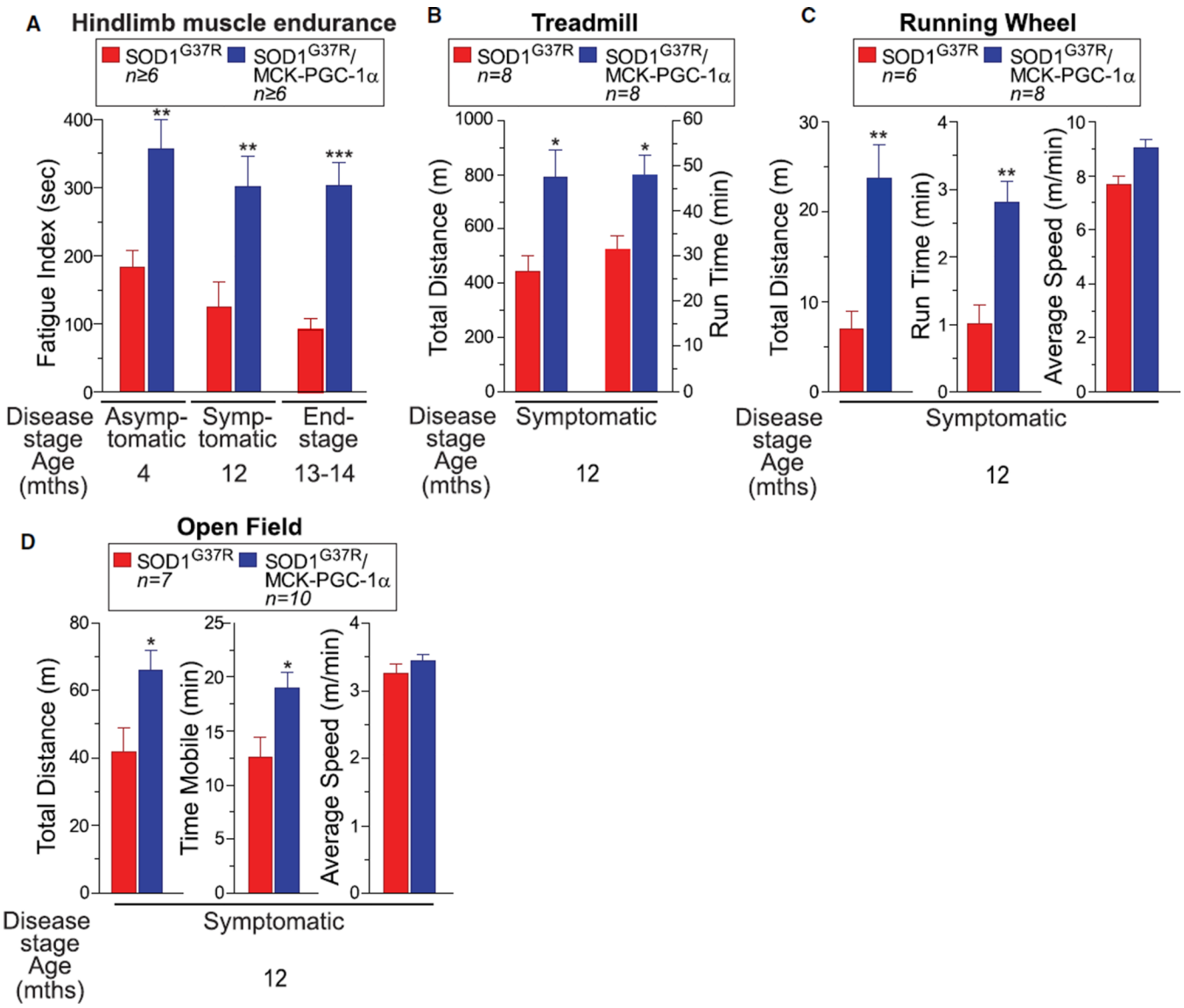

Figure 2. Elevating PGC-1α Expression Improves Muscle Activity and Locomotive Activity in Mutant SOD1^{G37R} Mice

(A) Fatigue index of hindlimb muscles from SOD1^{G37R} and SOD1^{G37R}/MCK-PGC-1α animals throughout disease. Fatigue index was quantified as the period (in seconds) of high-frequency electrical stimulation required to obtain a 50% decrease in muscle contraction. Data are presented as mean ± SEM. See also Figure S2.

(B) Treadmill performance (total distance and run time on the treadmill determined until exhaustion) of SOD1^{G37R} and SOD1^{G37R}/MCK-PGC-1α animals at the symptomatic stage of disease. Data are presented as mean ± SEM.

(C) Running wheel performance of SOD1^{G37R} and SOD1^{G37R}/MCK-PGC-1α animals at the symptomatic stage of disease. Total distance and run time on the wheel were determined during a 5 min testing period. Average speed corresponds to the mean speed of running during the mobile period. Data are presented as mean ± SEM.

(D) Open field performance of SOD1^{G37R} and SOD1^{G37R}/MCK-PGC-1α animals at the symptomatic stage of disease. Total distance covered and the time mobile were determined

during a 60 min of tracking period. Average speed corresponds to the mean speed of movement during the mobile period. Data are presented as mean ± SEM.

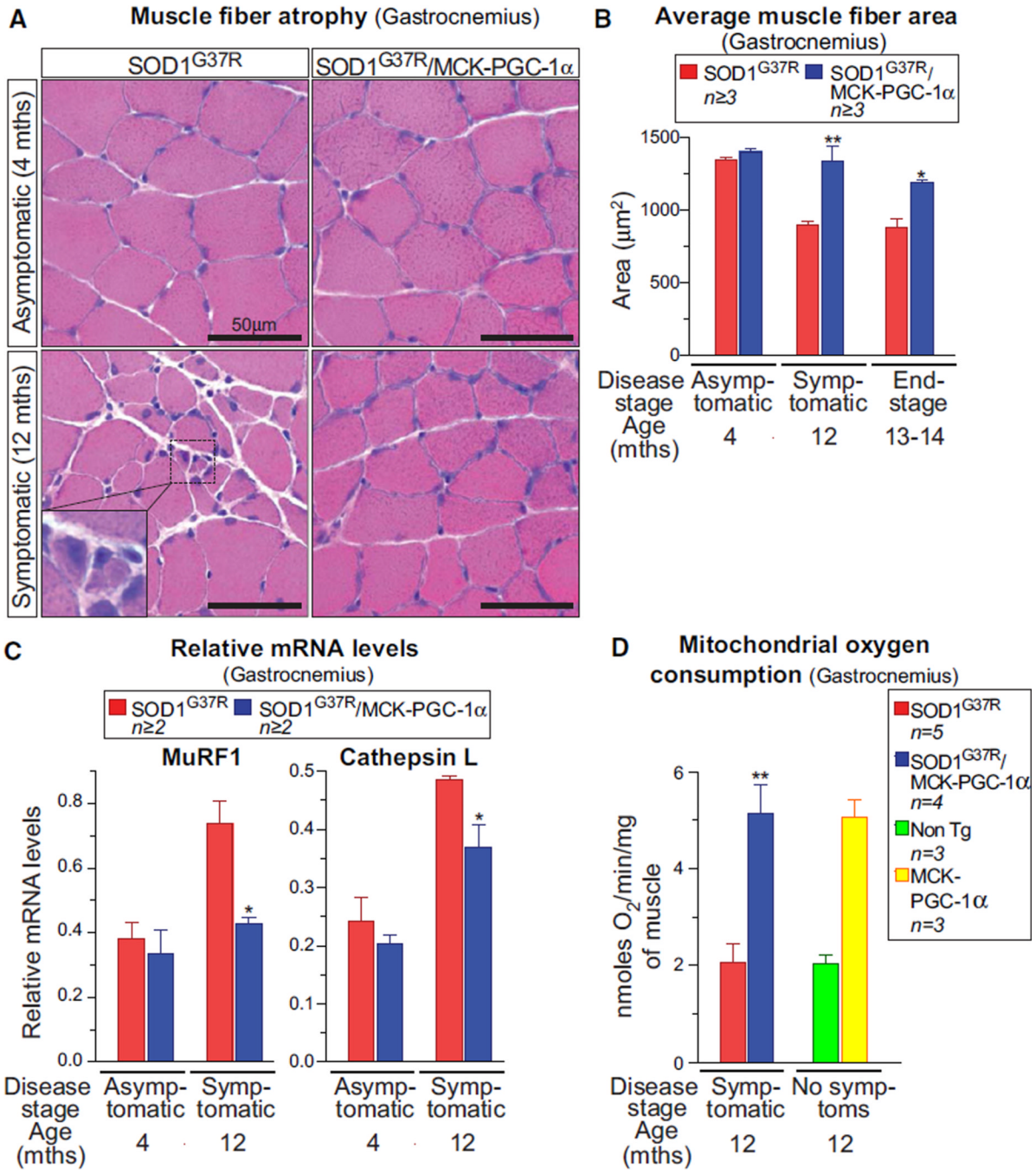

Figure 3. Elevating PGC-1α Expression Reduces Muscle Atrophy and Expression of Muscle Degeneration Genes and Increases Overall Muscle Mitochondrial ADP Phosphorylation Capacity in Mutant SOD1^{G37R} Mice throughout Disease

(A) Representative hematoxylin and eosin stainings of the gastrocnemius muscle in asymptomatic and symptomatic SOD1^{G37R} and SOD1^{G37R}/MCK-PGC-1α animals. The inset indicates clusters of small angular degenerating fibers.

(B) Quantification of average fiber area from hematoxylin and eosin-stained gastrocnemius muscle from SOD1^{G37R} and SOD1^{G37R}/MCK-PGC-1α animals throughout disease. Data are presented as mean ± SEM. See also Figure S3.

(C) Relative mRNA expression levels of muscular degeneration markers MuRF-1 and cathepsin L in gastrocnemius muscle isolated from asymptomatic and symptomatic mutant $SOD1^{G37R}$ and $SOD1^{G37R}$/MCK-PGC-1α animals. mRNA expression was evaluated by quantitative real-time PCR. Data are presented as mean ± SEM.
(D) Levels of ADP-stimulated mitochondrial oxygen consumption in mitochondria isolated from the gastrocnemius muscle of symptomatic mutant $SOD1^{G37R}$ and $SOD1^{G37R}$/MCK-PGC-1α and age-matched nontransgenic and MCK-PGC-1α animals oxidizing pyruvate and malate. In coupled mitochondrial respiration, oxygen consumption is directly proportional to the amount of ATP synthesized. Data are presented as mean ± SEM.

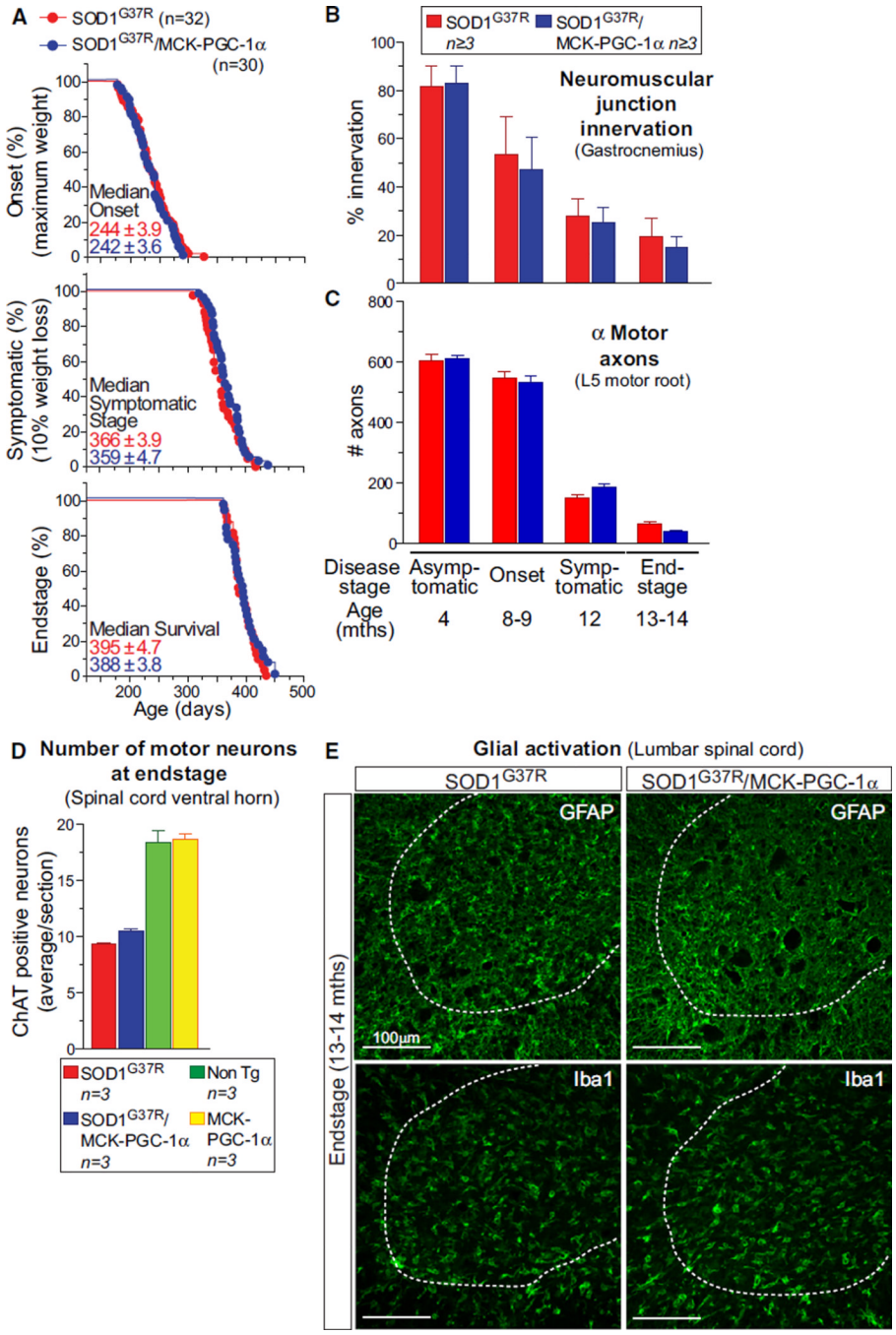

Figure 4. Elevating PGC-1α Expression in Skeletal Muscle of SOD1^{G37R} Mutant Mice Does Not Alter ALS Disease Course or Pathogenesis

(A) Plot of ages (in days) at which disease onset (as determined by the weight peak; at onset, animals do not display any obvious motor phenotype), symptomatic stage (as determined by 10% weight loss from onset, a stage characterized by clear gait abnormalities and tremor) and end-stage (as determined by hindlimb paralysis and inability to right itself) were reached for SOD1^{G37R} (red) and SOD1^{G37R}/MCK-PGC-1α (blue) animals.

(B–D) Quantification of innervation at the neuromuscular junction of the gastrocnemius muscle (B), total number of α-motor axons in the lumbar L5 motor root (C), and quantification at disease end-stage of the average number of large cholinergic ventral horn

motor neurons per section of lumbar spinal cord from $SOD1^{G37R}$ and $SOD1^{G37R}$/MCK-PGC-1α animals (D). Data are presented as mean ± SEM. See also Figure S4 for representative sections of the spinal cords used for quantification.
(E) Representative micrographs of lumbar spinal cord sections from $SOD1^{G37R}$ and $SOD1^{G37R}$/MCK-PGC-1α animals at disease end-stage processed for immunofluorescence using antibodies detecting activated astrocytes (GFAP) or microglia (IbaI). Dashed outlines correspond to the boundary between gray and white matter.